ACKNOWLEDGMENTS

We thank the many persons at APL/JHU, the Universities of Maryland and Kansas, and Bell Laboratories for their efforts in the design, fabrication, and implementation of the LECP experiment. We are especially grateful to the LECP coinvestigators, T. P. Armstrong, W. I. Axford, C. O. Bostrom, C. Y. Fan, G. Gloeckler, E. P. Keath, and L. J. Lanzerotti, for their contributions to the hardware and analysis efforts, and to our coauthors in previous publications, J. F. Carbary, D. C. Hamilton, and R. D. Zwickl, whose efforts were essential to the overall success of the data reduction and analysis. The efforts of Voyager project personnel at JPL and at NASA Headquarters were essential to the success of the LECP program. This analysis has been supported at APL/JHU by NASA under Task I of Contract N00024-78-C-5384 between The Johns Hopkins University and the Department of the Navy and by NASA Grant NAGW-154 to The Johns Hopkins University.

5
HIGH-ENERGY PARTICLES

A. W. Schardt and C. K. Goertz

In the Jovian magnetosphere, electrons, protons, and heavier ions are accelerated to energies well above 10 MeV. These energetic particles constitute a valuable diagnostic tool for studying magnetospheric processes and produce the Jovian radio emissions. In the inner magnetosphere, both the electron and proton fluxes with energies above 1 MeV build up to $\sim 10^8$ per cm^2 s and constitute a major radiation hazard to spacecraft passing through this region. Surprisingly, high fluxes of energetic oxygen and sulfur (>7 MeV/nuc) are also found in the inner magnetosphere. Of particular interest are the interactions of these particles with the inner Jovian moons and with the Io plasma torus. Throughout much of the middle magnetosphere and magnetospheric tail, highest fluxes are found in the plasma sheet, which coincides closely with the tilted dipole equator out to 45 R_J (Jupiter radii). This plasma sheet has not been identified beyond 45 R_J in the subsolar hemisphere; however, on the night side, it extends to 200 R_J. On the day side, fluxes near the equator are relatively independent of distance (15 to 45 R_J) and fall into the range 10^4 to 10^3 per cm^2 s each for protons and electrons above ~ 1 MeV. In the predawn direction, proton and electron fluxes decrease by three orders of magnitude from 20 to 90 R_J (10^5 to 10^2 per cm^2 s) and then remain relatively constant to the boundary layer near the magnetopause. In the middle and outer magnetosphere, particle fluxes change rapidly (2 to 10 min.), and it appears that the energetic particle population is subject to a number of different dynamic processes. Jupiter is a strong source of interplanetary electrons and $\sim 10^{14}$ W are required to energize these electrons. The electron flux above 2.5 MeV in interplanetary space and in large regions of the outer magnetosphere is modulated by Jupiter's rotation period. This modulation has been ascribed to the interaction of the solar wind with a rotating longitudinal asymmetry within the Jovian magnetosphere.

5.1. Introduction

Jupiter, as the biggest planet in the solar system, also has the largest magnetosphere. In many respects this magnetosphere is quite different from that of the Earth:

1. The energy required to drive the Jovian magnetosphere is apparently extracted from Jupiter's rotational energy rather than from the solar wind as is the case for the equivalent terrestrial system. In this sense, Jupiter, as a rapid rotator (Chap. 10), may serve as a laboratory for the study of pulsar physics.
2. The Jovian magnetosphere contains several satellites and a ring that not only absorb energetic particles, but are also a source of plasma that significantly affects the structure and dynamics of the Jovian radiation belts.
3. Jupiter is a strong source of energetic charged particles that can be detected as far away as the orbit of Mercury and that carry away energy at a rate of several million megawatts (much more than the present energy consumption of terrestrial civilization). Studying Jupiter may, hence, throw some light on astrophysical acceleration processes.

On the other hand, similarities also exist with the terrestrial magnetosphere. In fact, it is surprising how successfully concepts derived from the study of the Earth's magnetosphere have been applied.

Whereas fundamental magnetospheric properties are obtained from magnetic field and plasma data, energetic particles yield essential additional information. For the purpose of this chapter, energetic particles are defined as particles with an energy significantly higher than the "temperature" of the plasma. At Jupiter, this temperature may be as high as several tens of keV. Thus, particles with energies in excess of 0.5 MeV are mainly dealt with in this chapter. The lower-energy particles are described in Chapters 3 and 4. The energy density represented by the energetic particles is negligible compared to the energy densities of the plasma and magnetic field. Thus, they do not themselves affect the magnetic field, but are test particles that trace out field lines and, as such, yield information about the overall magnetic field topology. Energetic particles result from acceleration processes, and their characteristics help us to find the energization mechanisms that are active in the Jovian magnetosphere.

It has become traditional to divide the Jovian magnetosphere into distinct spatial regions, defined either by their special magnetic field properties, particle distributions or combinations thereof. The terms "inner," "middle," and "outer magnetosphere" are generally accepted (Fig. 5.1*a*). Usually, the boundaries between these are placed at 10–20 R_J and 30–45R_J, respectively.

There is little evidence for a well-organized current sheet throughout the front side of the outer magnetosphere, and no strong periodic modulation of the proton population has been observed, but an apparent 10-hr clocklike modulation of >6-MeV electrons was found. The azimuthal drift velocity is highly variable, being some of the time (but not always) lower than that expected from corotation.

The dawnside outer magnetosphere is characterized by a well-developed thin current sheet and open field lines relatively close to the current sheet. In many ways it resembles the Earth's magnetotail. Very close to the magnetopause it becomes similar in character to the front-side outer magnetosphere. Evidence for rapid local acceleration has been found in the taillike region. It is very likely that the energetic particles produced in the Jovian magnetosphere are released through the tail into interplanetary space.

The middle magnetosphere is characterized by the presence of a distinct azimuthal current sheet which becomes increasingly important at larger radial distances. The local-time asymmetry is less pronounced than in the outer region. The subsolar current sheet is much thicker than in the dawn region. On the day side, the orientation of the current sheet is predominantly rotationally controlled, whereas in the dawn magnetotail the current sheet evolves at larger distances into the more solar-wind-controlled configuration. In this middle region, field-aligned proton streaming has been observed. The proton phase space density changes little with distance, indicating that this region may be a source for these particles. Acceleration by magnetic pumping (Chap. 10) presumably occurs here. Evidence for the recirculation model (Chap. 10) is also strongest here. The azimuthal drift velocity is generally lower than that expected from corotation.

The inner magnetosphere (<15 R_J) is the best understood region. Whereas the properties of the outer magnetosphere depend sensitively on local time, very little of such a dependence is discernible in the inner magnetosphere. Except for the presence of the Galilean satellites, this region resembles the radiation belts of the earth. Energetic particles are transported inward by radial diffusion, gaining energy through adiabatic compression effect. They are pitch-angle scattered by electromagnetic waves and absorbed by the satellites and ring. As the electrons diffuse closer to the planet and, consequently, become more energetic, they begin to radiate significant amounts of synchrotron radiation, the decimetric radio emission observed at Earth. Particles scattered into the atmosphere cause auroral activity.

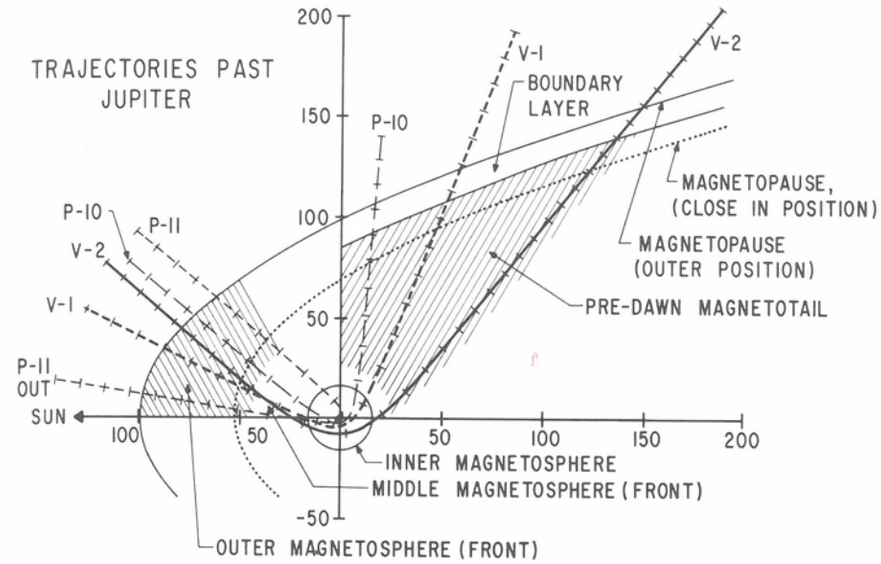

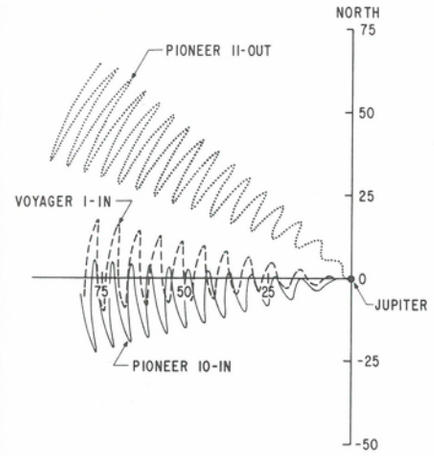

Fig. 5.1. Jupiter encounter trajectories: (*a*) Distance from Jupiter plotted at its local time or azimuth relative to the Sun–Jupiter line. Pioneer 10 and 11 trajectories are designated with P-10 and P-11; similarly, the Voyager 1 and 2 trajectories by V-1 and V-2. Tick marks indicate the start of a new day, and the two magnetopause positions shown correspond to high and low solar wind pressure; (*b*) Magnetic dipole coordinates of representative Pioneer and Voyager trajectories.

The data described here come from four flybys whose trajectories are shown in Figure 5.1*a*. The local-time coverage in the middle and outer magnetospheres is incomplete, extending only from 2:00 to 14:00 (Fig. 5.1*a*). For energetic particles, the magnetic latitude of the spacecraft is the other important parameter. Due to the offset between the spin axis and the magnetic dipole axis, the dipole latitude (Fig. 5.1*b*) oscillates around the geographic latitude by about $\pm 10°$ every 9 hr 55 min. Because the actual magnetic field deviates from a dipole in the middle and outer magnetospheres, Figure 5.1*b* represents only a first approximation. Particle flux modulations with this period are primarily due to latitudinal effects; however, a given latitude is encountered only at two longitudes and only once at the extremes. Therefore, the available data do not permit a unique separation between latitudinal and longitudinal effects. These limitations are unavoidable with flybys and can only be removed by a Jupiter orbiter.

Of all the properties of the Jovian magnetosphere, the characteristics of the energetic particles have been measured most extensively. Table 5.1 lists the instru-

Table 5.1. *Energetic particle detectors*

Group	Designation	Particle sensitivity	Energy range (MeV)	Spacecraft
University of Chicago Simpson et al., 1974a	ECD	Electrons Protons	> 3 > 30	Pioneer 10,11
	Fission Cell	Protons Electrons α Heavy Nuclei	> 35	Pioneer 10,11
	LET	Protons He^{++}	0.54 – 8.8 0.30 – 5.0	Pioneer 10,11
University of Iowa Van Allen et al., 1974a	GNA	Electrons Protons	> 5 > 30	Pioneer 10,11
	GMB	Electrons Protons	> 0.55 > 6.6	Pioneer 10,11
	GMC	Electrons Protons	> 21 > 77.5	Pioneer 10,11
	GMD	Electrons Protons	> 31 > 77.5	Pioneer 10,11
	GMG G	Electrons Protons	> 0.06 0.61 – 3.4	Pioneer 10 Pioneer 11
University of California at San Diego (UCSD) Fillius and McIlwain, 1974a	C1	Electrons	> 6 > 5	Pioneer 10 Pioneer 11
	C2	Electrons	> 9 > 8	Pioneer 10 Pioneer 11
	C3	Electrons	> 13 > 12	Pioneer 10 Pioneer 11
	M1	Electrons	> 35	Pioneer 10,11
	M2	Background	> 0.85	Pioneer 10,11
	M3	Protons	> 80	Pioneer 10,11
GSFC/University of New Hampshire Trainor et al., 1974	HET	Electrons Protons and He^{++} Medium Nuclei	2.1 – 8.0 MeV 20 – 500 MeV/nucl. 40 – 120 MeV/nucl.	Pioneer 10,11
	LET I	Protons Protons and He^{++} Medium Nuclei	0.4 – 3 MeV 3 – 21 MeV/Nucl. 6 – 40 MeV/nucl.	Pioneer 10,11
	LET II	Electrons Protons plus Ions Protons	0.05 – 2.1 MeV 0.2 – 2.1 MeV 3.2 – 21 MeV	Pioneer 10,11

Table 5.1. *(cont.)*

Group	Designation	Particle sensitivity	Energy range (MeV)	Spacecraft
CALTECH/GSFC Cosmic Ray System (CRS) Stone et al., 1977	LET	Protons and He^{++} Medium Nuclei	0.43 – 8 MeV 7 MeV/nucl.	Voyager 1,2
	HET	Electrons	0.1 – 12 MeV	Voyaber 1,2
	TET	Electrons	> 0.6 MeV	Voyager 1,2
Applied Physics Lab (APL) Low-energy Charged Particle Krimigis et al., 1977	LECP	Electrons Ions (mainly concerned with low-energy particles)	0.014 – 10 MeV 0.030 – 150 MeV	Voyager 1,2

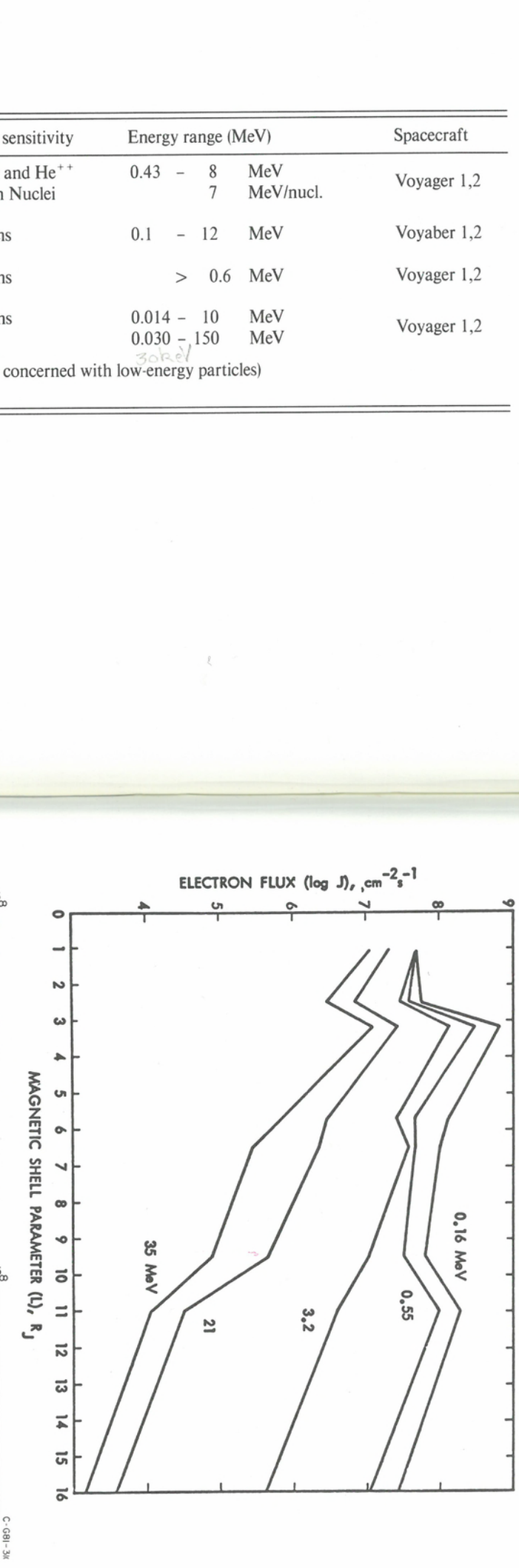

Fig. 5.2. Omnidirectional integral electron flux above several threshold energies: (*a*) Radial dependence according to the Divine (1976) model (reprinted with the permission of Divine [1976] and the Jet Propulsion Laboratory). (*b*) and (*c*) Comparison between the Divine (1976) model, solid line, and observations by the University of Iowa detector, dots [from Thomsen, 1979].

ments that have provided the data on which this chapter is based. For details of the instruments, for example, their ability to distinguish species and resolve pitch angle distribution and time variations, we refer the reader to the original literature.

In view of the accessibility of the original literature (see Preface), and in the interest of readability, we will not refer to all original papers but use their results freely.

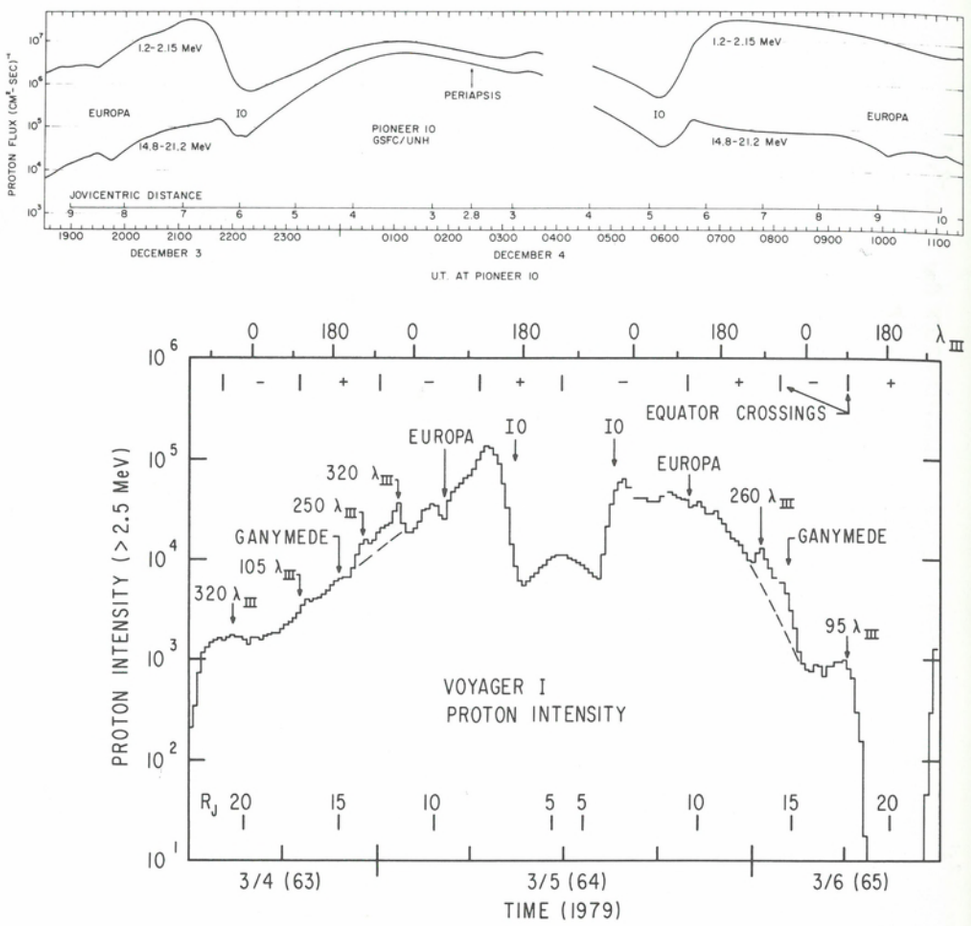

Fig. 5.3. (*a*) Omnidirectional, integral proton flux observed with the Goddard space Flight Center/University of New Hampshire (GSFC/UNH) experiment on Pioneer 10, showing the intensity variations at the orbits of Io and Europa [from Trainor et al., 1974]. (*b*) Relative proton intensities (16-min. averages) observed in the inner magnetosphere with the Voyager 1 experiment of the California Institute of Technology/Goddard Space Flight Center (CIT/GSFC). Owing to large deadtime corrections, the magnitude of the drop at Io is uncertain, and the detector threshold increased with counting rate. Equatorial crossings are indicated with tick marks and the + indicates when Voyager 1 was in the northern hemisphere.

5.2. Inner magnetosphere ($R < 15\ R_J$)

In discussing the structure and dynamics of the energetic particle distribution, there are four important questions to be answered:

1. How many particles are there?
2. How are they transported?
3. What are the losses they suffer as they are transported?
4. What, finally, is their source?

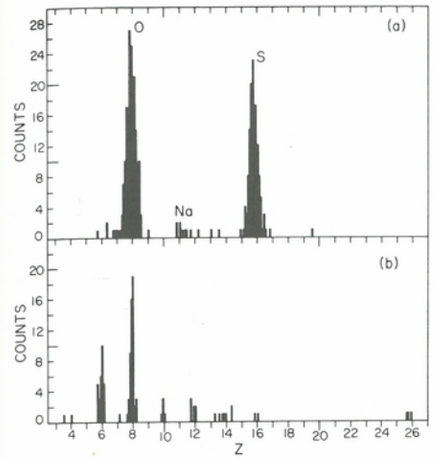

Fig. 5.4. Elemental (Z) distribution of heavy nuclei observed with Voyager 1 in the Jovian environment (CIT/GSFC experiment). The energy was ≥ 7 MeV per nucleon: (*a*) Within 5.8 R_J inside Io's orbit, (*b*) Outside 11 R_J [From Vogt et al., 1979a].

Observations

The first question has been fairly well answered by observations obtained during the four flybys. Although the list of instruments from which measurements are available is quite impressive (Table 5.1), few of these instruments provided unambiguous data in the very intense radiation levels of the inner magnetosphere. There are problems with penetrating background radiation, decreased efficiency and dead-time uncertainties. Particle species identification and absolute intensity levels are, thus, not always completely reliable; however, the experimenters have, to a large extent, corrected for these problems and, due to the energy overlap of different instruments, a fairly coherent picture has emerged.

A few years after the Pioneer 10 and 11 encounters, several authors [Divine, 1976, unpublished, 1978; Mihalov, 1977] combined the data from different instruments into time-stationary models of the distribution of energetic particles. Figure 5.2*a* shows the empirical model produced by Divine. Figures 5.2*b* and 5.2*c* show the comparison of the model with observed omnidirectional intensities of electrons with energies $E > 21$ MeV and $E > 31$ MeV. Clearly, for these high energies, the model fits the data quite well; however, the fit at lower energies is much less impressive. This discrepancy is probably due to larger time-variability of low-energy fluxes. It seems that the success of the time-stationary Divine and Mihalov models in fitting the energetic electron data indicates that there exists a steady long-term average electron distribution about which temporal fluctuations occur. The amplitude of the fluctuations decreases with increasing energy. Although no detailed comparisons of Voyager 1 and 2 data with the Divine or Mihalov models are available as yet, it appears that the general flux level of electrons above 1 MeV did not change significantly between the Pioneer and Voyager encounters. This is an agreement with the observed long-term stability of decimetric radiation.

Figures 5.3*a* and *b* show the radial variation of the intensity of energetic ions in the inner region obtained from different instruments on different flybys. Whereas the Pioneer data were always interpreted in terms of protons being the dominant ion, it has become apparent since the Voyager encounters that energetic sulfur and oxygen ions are also quite significant. Figure 5.4 shows the masses of heavy ions with energies ≥ 7 MeV per nucleon. They reflect the solar composition in the outer magnetosphere, but only oxygen, sulfur and, to a lesser degree, sodium are present in the inner region

[Vogt et al., 1979a]. (See Chap. 4 for a discussion of ion fluxes with energies below 7 MeV/nuc.) Krimigis [1979, private communication] has pointed out that the Pioneer data may be due in part to heavier ions and that the absolute intensity levels of "protons," as derived from Pioneer data, are difficult to obtain.

Figures 5.2 and 5.3 display similarities, but also significant differences. Both ions and electrons increase in intensity with decreasing distance. This has been interpreted as a signature of inward radial diffusion. For both electrons and ions the energy spectrum becomes harder with decreasing radial distance. This may also be a result of radial diffusion. The ions are much more affected by the satellite Io and its plasma torus than the energetic electrons. (This is not necessarily true for lower-energy particles.) This difference has been interpreted as being the result of reduced access of energetic electrons to Io and enhanced pitch angle scattering of ions in the plasma torus (see section on Satellite Interactions). Near Europa, the electron and ion signatures are more similar because of the absence of a plasma torus.

Our knowledge of the pitch angle distributions of the energetic particles in the inner region is less complete than our knowledge of their spatial and energy distributions, in part because the response of a number of the high-energy detectors is omnidirectional and the overlap in energy coverage is reduced. Conflicting results have been published regarding the nature of the proton pitch angle distribution outside Io's orbit. The University of Chicago group [Simpson et al., 1974a] report dumbbell proton distributions (peaked at $\sim 0°$ pitch angle) outside of $L = 6$, which change dramatically to pancake distributions (peaked at $\sim 90°$ pitch angles) at Io's orbit. Other instruments on Pioneers 10 and 11 did not see dumbbell distributions in the region outside of Io's orbit, but rather pancake distributions. A pancake distribution was also observed with Voyager [Lanzerotti et al., 1981]. However, the pancake distributions do become more pronounced inside of Io's orbit. Note that this is true only for the energetic particles discussed here. For lower-energy ions, the reverse is true. Lower-energy ions are depleted near 90° inside Io's orbit, which could be due to charge exchange [Lanzerotti et al., 1981].

The electron pitch angle distributions are pancake throughout the inner magnetosphere, with the pancake nature becoming more pronounced with decreasing radial distance. At the orbit of Io, the trend towards more sharply peaked distributions is halted. Inside of Io's orbit, the sharpness of the pancake distribution of $E_e > 9$-MeV electrons remains constant. There is even some indication for a decrease at the orbit of Io [Fillius, 1976]. This is not an unexpected signature for absorption of charged particles by a moon.

Transport and losses in the inner magnetosphere

Before the flybys of Pioneer 10 and 11, the theoretical discussion of the structure of Jupiter's (inner) magnetosphere centered on the question of diffusive transport and on the probable loss mechanisms that would operate on the trapped energetic particles. It was recognized that a solar wind-driven convection would not extend into the inner regions of the Jovian magnetosphere and that radial diffusion was proposed as the most likely transport mechanism [Brice and McDonough, 1973]. Regarding loss mechanisms, considerable attention was paid to the role of wave-particle interactions as a mechanism for causing pitch angle scattering of particles into the loss cone [Thorne and Coroniti, 1972].

The Pioneer flybys obtained experimental evidence from the energetic particle data to support the theoretical expectations that pitch angle diffusion significantly affects

the energetic charged particles in the inner magnetosphere, and the intensity and frequency spectrum of waves responsible for the pitch angle diffusion were estimated [Sentman and Goertz, 1978]. These waves have now been observed in situ by plasma wave instruments on board Voyager 1 and 2 (Chaps. 8 and 12). It was also realized that the particles precipitating into the Jovian ionosphere would deposit a significant amount of energy and could give rise to a number of possible effects, including ionospheric heating, plasma loading of the magnetosphere due to the production of secondary electrons that can escape the gravitational potential barrier, and optical and x-ray emissions. Both optical (auroral type) and x-ray emission from the Jovian ionosphere have recently been found (Chaps. 2 and 6). Auroral emission has been observed to come preferentially from the foot of the magnetic field lines threading the Io plasma torus. It has been argued by several authors that there should be enhanced wave activity and, consequently, enhanced pitch-angle scattering into the atmospheric loss cone in the Io torus. Such an enhanced wave activity is, indeed, observed (Chaps. 8 and 12). Considering the potential complexity of the problem, the list of successful predictions is quite impressive.

The theoretical model, on the basis of which many of the predictions were made, had been developed to explain the structure of the earth's radiation belts. It is gratifying, indeed, to find that the model is also applicable to the Jovian magnetosphere. The starting point of the analysis is the equation for radial diffusion in the magnetic field of the planet with conservation of the first and second adiabatic invariants

$$\frac{\partial f}{\partial t} = L^2 \frac{\partial}{\partial L}\left(\frac{D_{LL}}{L^2}\frac{\partial f}{\partial L}\right) - \mathscr{L} + S \tag{5.1}$$

In Equation (5.1), f is the phase space density of particles with first and second invariant μ and J_2; it is related to the "measured" differential unidirectional particle flux per cm^2 sr s, by the expression

$$f(\mu, J_2, L) = \frac{dN}{d^3 \times d^3 p} = \frac{j(E, \delta_o, L)}{p^2} \tag{5.2}$$

where

$$E = E(\mu, J_2, L) = \text{particle kinetic energy} \tag{5.3a}$$

$$\delta_o = \delta_o(\mu, J_2, L) = \text{equatorial pitch angle} \tag{5.3b}$$

and

$$p^2c^2 = E^2 + 2E m_o c^2 \tag{5.3c}$$

The variable L is the normal L-shell parameter which in the complex magnetic field of Jupiter depends on the particle's energy and pitch angle. D_{LL} is the diffusion coefficient. Usually one assumes a parametric form $D_{LL} = D_o L^n$. The symbols $\mathscr{L}$ and S represent loss and source terms, and the assumption of steady state ($\partial f/\partial t = 0$) is made, which is probably valid for high-energy particles in the inner magnetosphere. The loss and source terms are often combined and written as

$$\mathscr{L} - S = f/\tau \tag{5.4}$$

where $\tau(\mu, J_2, L)$ is a characteristic lifetime of particles. This combined loss and source term (note that τ may be negative if sources exceed losses) is comprised of a number of possible processes: pitch-angle diffusion, satellite sweep up, satellite injection, interparticle collisions, synchrotron radiation, etc. It is not clear that each physical process can be represented by a form like Equation (5.4); however, the obvious mathematical advantages of Equation (5.4) have generally outweighed such doubts. Combining Equations (5.4) and (5.1) and assuming that the particle population does not change ($\partial f/\partial t = 0$), we arrive at what has become known as the "lossy radial diffusion model,"

$$L^2 \frac{\partial}{\partial L}\left(\frac{D_{LL}}{L^2}\frac{\partial f}{\partial L}\right) - f/\tau = 0 \tag{5.5}$$

The analysis of the particle data in the framework of this model has proceeded in two ways: One either assumes a loss rate and determines the diffusion coefficient or vice versa.

Satellite interactions

An example of the first method is the analysis of the particle flux profile as the spacecraft crosses the orbit of a Jovian moon [for details see Mogro-Campero, 1976, and Thomsen, Goertz, and Van Allen, 1977a,b]. The characteristic loss time for absorption by a moon sweeping the region between L_1 and L_2 is given by

$$\tau = \frac{3}{2}\frac{t_s(\Delta L/r_m)}{\alpha_L\,\alpha_D} \tag{5.6}$$

where ΔL is the range of L values covered by the moon's orbit and r_m is its effective radius (Chap. 11). The value of ΔL depends on the eccentricity of the satellite's orbit, the magnetic field topology and the particle's energy and pitch angle. A complete treatment must take into account factors such as L-shell splitting in order to evaluate the L values along the moon's orbit in a nondipolar magnetic field. The time t_s is the time between two successive encounters of a particle with the moon. If ω_C, ω_D, and ω_m are the angular velocities of corotation, of magnetic curvature and gradient drifts, and of the moon, respectively, we have

$$t_s = \frac{2\pi}{\omega_C - \omega_m \pm \omega_D} \tag{5.7}$$

The plus sign is for positive particles and the minus sign is for electrons. For the inner moons like Io, ω_C is equal to Jupiter's angular velocity. If a particle's mirror latitude is less than the moon's magnetic latitude, it can escape absorption. The factor α_L is the fraction of a moon's orbit where this is the case.

If the drift velocity and bounce period of the particles are such that in one-half bounce period they would drift more than one moon's diameter relative to the satellite, then some particles may escape absorption by "leapfrogging" over the satellite. This effect is represented by α_D, which is the fraction of particles in a given flux tube which are absorbed in one encounter of the moon with the flux tube [for details see Thomsen, Goertz, and Van Allen, 1977a,b].

The effective satellite radius r_m depends on electric and magnetic field perturbations in the vicinity of the satellite. τ may be poorly known because it is not easy to determine r_m a priori. Analysis of the energy dependence of τ for different models of the electric fields in Io's vicinity [Thomsen, 1979] shows that little can be said with certainty about τ and, hence, about D. Published estimates of τ and D are based on modeling the moons with spherical absorbers of infinite resistivity. In this model r_m is equal to the particle's cyclotron radius plus the moon's radius; however, the reader should keep in mind the drastic assumptions underlying the model. In that case, one finds for protons of $\mu = 1.7$ MeV/G at $L \simeq 6$, a value for $\tau = 1.1 \times 10^6$s. Outside the range from L_1 to L_2, the losses are usually assumed to be small, that is,

$$0 \quad L < L_1 \qquad \text{region I}$$

$$\frac{1}{\tau} = \frac{1}{\tau} \quad L_1 \le L \le L_2 \qquad \text{region II}$$

$$0 \quad L > L_2 \qquad \text{region III}$$

Requiring continuity of f and its derivative at L_1 and L_2, one can solve Equation (5.1) and fit the solution to the observed phase space density profiles in the vicinity of a moon. The L dependence of D_{LL} near the moon's orbit may be neglected.

Figure 5.5*a* shows examples of such calculations at the moon Io ($L = 5.9$). We see that a reasonable fit can be obtained; however, the proton data require that $D = 2.6 \times 10^{-8}\,R_J^2\,s^{-1}$, while the electron data are consistent with $D = 4 \times 10^{-7} R_J^2\,s^{-1}$. The difference is unexpected on theoretical grounds. The rapid change in proton phase-space density extends over a larger radial range than specified as Region II in Figure 5.5*a*, and a better fit is obtained for a larger sweeping region as shown in Figure 5.5*b*. Because the sweeping range $5.6 \le L \le 6.4$ is much larger than the range covered by Io, the losses of protons may not be entirely due to absorption by Io but also due to pitch angle scattering in a toruslike region of enhanced plasma density (Chap. 3). Using a minimum scattering lifetime, Thomsen, Goertz, and Van Allen [1977a] estimated an upper limit for the diffusion coefficient in Io's torus of $D = 1.5 \times 10^{-7}\,R_J^2\,s^{-1}$. For a combination of pitch angle scattering and Io absorption, the diffusion coefficient is $D = 6 \times 10^{-7} R_J^2\,s^{-1}$ in good agreement with the value obtained from the electrons. Other estimates for D range from $10^{-9}\,R_J^2\,s^{-1}$ for protons to $10^{-6}\,R_J^2\,s^{-1}$ for electrons [Simpson et al., 1974a]. Mogro-Campero and Fillius [1976] found $D = 6 \times 10^{-8}\,R_J^2\,s^{-1}$ or $D = 3 - 4 \times 10^{-7} R_J^2\,s^{-1}$, depending on the analysis method they used.

To obtain a value for the exponent n in the variation of $D_{LL} = D_o L^n$, one can go through the same exercise at other moons, for example, Europa. This indicates that n is probably less than 6, most likely even less than 4. One can also use the shape of the phase space density profile in Regions I and III to determine n. From the proton data, one obtains $n = 2.3 \pm 0.5$, which is more consistent with diffusion coefficients theoretically derived by assuming that the radial diffusion is driven by ionospheric dynamo fields than by assuming fluctuating solar wind-driven convection electric and magnetic fields. The reader must, however, be cautioned against an uncritical acceptance of this widely stated conclusion. The theoretically expected values of $n = 3, 7$–10 and $\simeq 10$ for the respective processes are all based on ad hoc assumptions concerning the fluctuation spectrum and its radial dependence. A recent determination of n using Voyager 1 and 2 data of >0.5-MeV ions by Armstrong et al. [198l] does not yield a low value of n but indicates a best value of $n \sim 7.5$. However, only 15 data points were

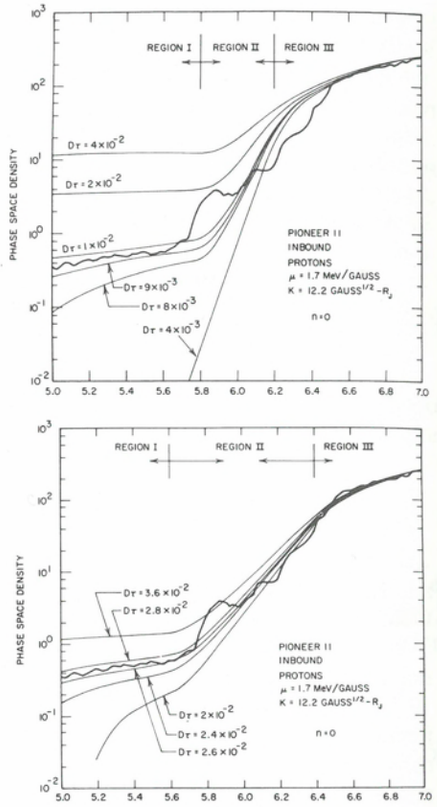

Fig. 5.5. Phase space density profile of protons with $N = 1.7$ MeV/G and $K = 12.2\, G^{1/2}\, R_J$ for the Pioneer 11 inbound trajectory (University of Iowa experiment). The heavy line shows the phase space density derived from observations, and the light lines show solutions as a function of the parameter $D\tau$ (in units of R_J^2). (*a*) The loss region is taken to be $5.8 \geq L \geq 6.2$. (*b*) An extended loss region is used, $5.6 \geq L \geq 6.4$ [from Thomsen et al., 1977a].

used; furthermore, the experimental data do not allow for an accurate determination of n because all loss processes are not properly known.

Using these estimates for the diffusion coefficient, one can fit phase space density profiles in regions remote from moons and obtain lifetimes τ, that is, loss rates. All authors have concluded that for energetic electrons the lifetime is not infinite, thus, local losses do occur. The total loss rate of energetic electrons ($E_e > 200$ keV) between $L = 10$ and $L = 3$ has been estimated by Thomsen and Sentman [1979] as 10^{24} particles/s. These particles, if precipitating into the Jovian atmosphere, would constitute a considerable amount of heating, namely a few tenths of a mW m^{-2}. The cause of these losses has been suggested to be pitch-angle scattering by resonant interaction with electromagnetic waves in the whistler mode. Indeed, such waves have been observed in the Jovian magnetosphere. For more detail about wave-particle interaction in the Jovian magnetosphere, we refer the reader to Chapter 9.

Electron synchrotron radiation

Inside $L \simeq 3$, loss due to synchrotron radiation becomes important. In fact, one can use the well known equations for synchrotron radiation to calculate τ in this region [see e.g., Birmingham et al., 1974]. The estimates for the diffusion coefficient obtained from balancing radial diffusion with synchrotron losses (observed decimetric, DIM, radiation from Jupiter) agree very well with the ones quoted above. Furthermore, the

DIM radiation intensities calculated from observed electron fluxes agree with observed values, confirming quite nicely the synchrotron radiation theory of DIM.

The observations of DIM are described in Chapter 7. DIM consists of two components: the thermal radiation from Jupiter's atmosphere and the nonthermal, or synchrotron, radiation. It is this second component which can be used to deduce the characteristics of the energetic particles and magnetic fields in the innermost region of the Jovian magnetosphere ($r \leq 3\, R_J$).

Recently, de Pater [198la,b] completed an elaborate model calculation for Jupiter's synchrotron radiation. The full multipole magnetic field configuration is used, as well as a realistic electron distribution in energy and pitch angle (see Chap. 7). Outside Amalthea's orbit, her particle distribution agrees well with Pioneer observations; however, inside this orbit, where no comprehensive data are available, the pitch angle distribution is considerably sharpened towards 90° pitch angles because only these particles can escape absorption by Amalthea. A similar effect occurs across the L shell of the newly discovered ring. These effects account for the observed degree of circular polarization and the sharp increase in the intensity of the radiation peaks near the ring.

Whereas the overall agreement between the calculated radiation parameters and the observed ones is good, certain observed features cannot be accounted for by the model. The conspicuous "hot spots" of the DIM radiation at longitudes $\lambda_{III} = 225° \pm 10°$ require a relative overabundance of energetic electrons at longitudes 240° to 360° and perhaps a dusk to dawn electric field in the inner magnetosphere. Conceivably, our knowledge of Jupiter's magnetic field is still inadequate to reproduce this detail; however, it should also be noted that longitudinal asymmetries are quite common in the Jovian magnetosphere and form the basis of what is commonly known as the "magnetic anomaly model" (see Chap. 10). It is quite likely that many diverse effects, including corotating convection driven by a surface magnetic anomaly, combine to cause specific asymmetries.

We summarize this section by stating that energetic particles in the inner magnetosphere are transported radially inward by a diffusive process. It seems that the diffusion is driven by ionospheric dynamo fields produced by winds in the atmosphere of Jupiter. The particles are subject to strong losses resulting from pitch angle scattering into the atmospheric loss cone by resonant cyclotron interaction with electromagnetic waves. The particles are also absorbed by the moons Europa and Io, although the efficiency of that process is poorly known. Inside $L \simeq 3$ synchrotron radiation (see Chap. 7) becomes an important loss mechanism for energetic electrons.

5.3. The subsolar hemisphere

The outer and middle magnetosphere show considerable variations with local time. The fact that there are differences, to be described below, in particle intensities, pitch-angle distributions, energy spectra, and modulation phase and amplitude cannot be stressed enough. Such differences indicate that the external influence of the solar wind is important for the outer and middle magnetosphere. Models that neglect azimuthal effects cannot claim to be realistic global models although they may work well over a limited range of local time. (Most quantitative models proposed to date apply only to a limited region of the magnetosphere. In light of our severely restricted local time coverage, global models must still be regarded as speculative.)

For energetic particles, the transition from the inner to the middle magnetosphere occurs at about 15 R_J because, beyond that distance, the magnetic field distortion affects the trapped energetic particles in a major way. The plasma sheet responsible for

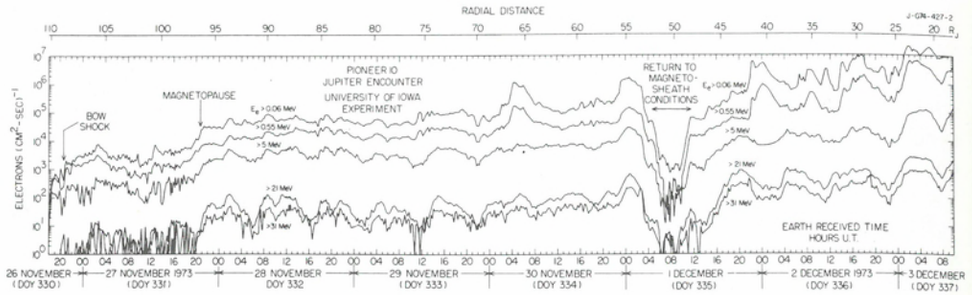

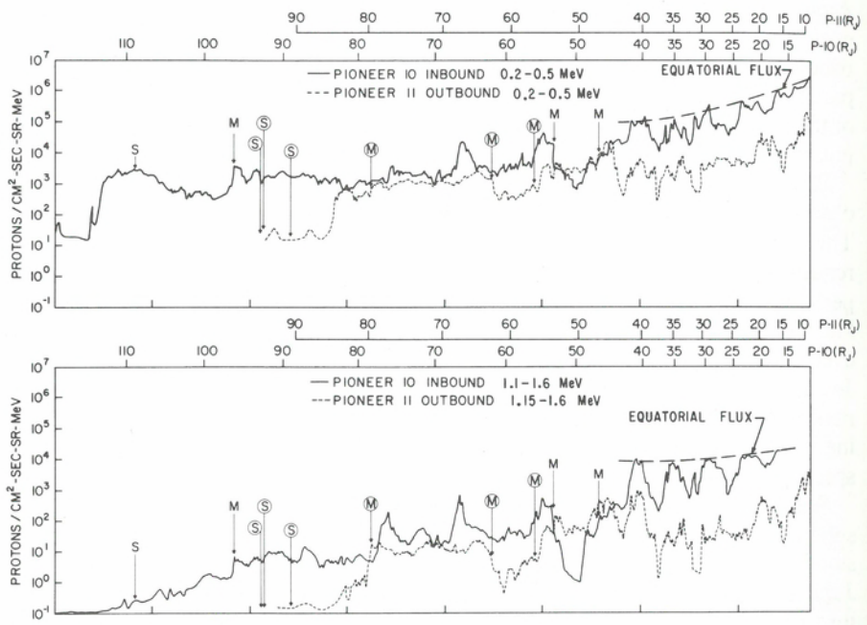

Fig. 5.6. Omnidirectional proton and electron fluxes observed with Pioneer: (*a*) Electron fluxes between 20 and 110 R_J observed on the inbound pass of Pioneer 10 with the University of Iowa Experiment [from Baker and Van Allen, 1976]. (*b*) Differential proton fluxes from the Pioneer 10-in and Pioneer 11-out passes. The bow shock and magnetopause crossings are indicated by arrows labeled S and M, respectively, with those for Pioneer 11 enclosed in a circle [from McDonald, Schardt, and Trainor, 1979; GSFC/UNH experiment].

the field distortion has been identified to only about 45 R_J in the subsolar hemisphere. Beyond 45 R_J, the plasma sheet is either absent or very thick in this hemisphere and cannot be identified by its magnetic field signature. The size of this region, called the outer magnetosphere, depends sensitively on solar wind pressure. The outer magnetosphere extends from 45 R_J to the magnetopause, which has been observed between the extremes of 46 and 97 R_J.

Particle fluxes in the subsolar magnetosphere

Electron and proton fluxes in the front magnetosphere are shown in Figures 5.6, 5.7, and 5.8. Generally, several magnetopause crossings are observed (Fig. 5.6*b*) as the size of the magnetosphere changes in response to variations in solar wind pressure. The

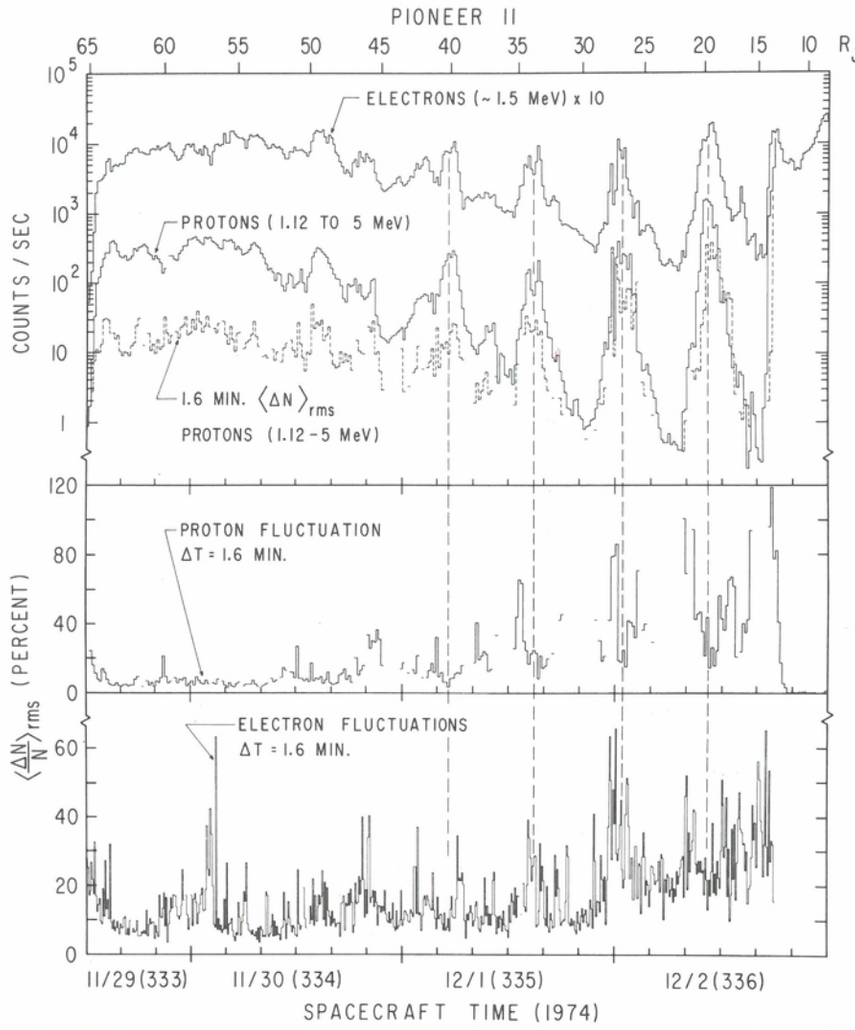

Fig. 5.7. Sixteen-minute averages of proton and electron intensities observed during the inbound pass of Pioneer 11 (GSFC/UNH experiment). Also given are the rms fluctuations, averaged over 16 min., of counting rates observed 1.6 min. apart. Fluctuations are shown only for periods during which the χ^2 test indicates a $>95\%$ probability that the fluctuations are not due to counting statistics.

average flux has little radial dependence; however, in the outer magnetosphere, fluxes of particles below 2 MeV have an irregular dependence on time and appear to respond primarily to changes in interplanetary conditions. In the middle magnetosphere, the wobble of the plasma sheet produces a strong periodic modulation, which is particularly well illustrated in Figure 5.7. As may be seen in Figure 5.1*b*, the Pioneer spacecraft entered the plasma sheet only once per Jovian period (~ 10 h) while the low-latitude Voyagers 1 and 2 crossed the plasma sheet twice. Accordingly, the Pioneer fluxes (Figs. 5.6 and 5.7) were modulated with a 10-hr period and the Voyager fluxes with a 5-hr period (Fig 5.8). Also, the Pioneer modulation is much deeper than observed with Voyager because of the larger latitude excursion (Fig. 5.1*b*). As may be

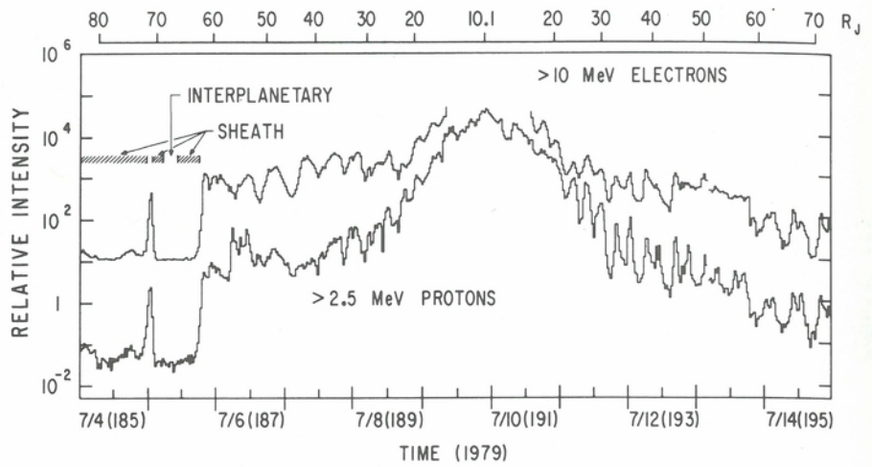

Fig. 5.8. Electron and proton intensities (32-min. averages) observed during the Voyager 2 encounter [from Vogt et al., 1979b; CIT/GSFC experiment].

seen in Figures 5.6*a* and 5.8, the 10-hr modulation of >5-MeV electrons persists in the outer magnetosphere. This modulation is due to a different mechanism than the one in the middle magnetosphere and will be discussed further as "clock" modulation.

Superimposed on the average fluxes are large-intensity fluctuations on a minute timescale. These fluctuations are illustrated in Figure 5.7 in terms of their rms values. Except for special periods, the percentage fluctuations became quite small (<3%) in the inner magnetosphere. Examples of larger fluctuations in the inner magnetosphere occurred near satellite orbits, for example, Ganymede [Burlaga, Belcher, and Ness, 1980; Connerney, Acuña, and Ness, 1981]. The existence of such rapid flux changes is indicative of dynamic processes in the middle and outer magnetospheres. Because little correlation exists between electron and proton fluctuations, different or spatially separate processes must affect the two types of populations.

Middle magnetosphere

The plasma sheet, which occurs near the magnetic dipole equator, has a dominant influence on the particle population in the middle magnetosphere. The approximately 10° tilt of the dipole relative to the Jovian spin axis caused the magnetic latitude of Pioneer 10 to oscillate between +1° and −19° and, hence, between regions of stronger and weaker particle fluxes. The Pioneer 11-out observations between 20 and 45 R_J extend the magnetic latitude range from 24° to 44°. As might be expected, the maxima in the Pioneer 11-out proton flux (Fig. 5.6*b*) are just slightly less than the minima in the Pioneer 10 flux; however, no such match was observed in the electron flux. The latitudes of Voyagers 1 and 2-inbound oscillate between +7° and −13°.

The approximate value of flux vs. distance at the equator is indicated by the dashed line in Figure 5.6*b*. It should be remembered, however, that Pioneer 10 inbound sampled the equatorial flux at only one system III (1965) longitude near $\lambda_{III} = 200°$. A longitudinal asymmetry in the energetic particle flux is a possible consequence of the magnetic-anomaly model (see Chaps. 10 and 11). Both the Voyager 1 and Pioneer 10-in data are consistent with a maximum flux in the active hemisphere. Voyager 1 crossed the magnetic equator twice each Jovian period near $\lambda_{III} = 100°$ and 310°, and

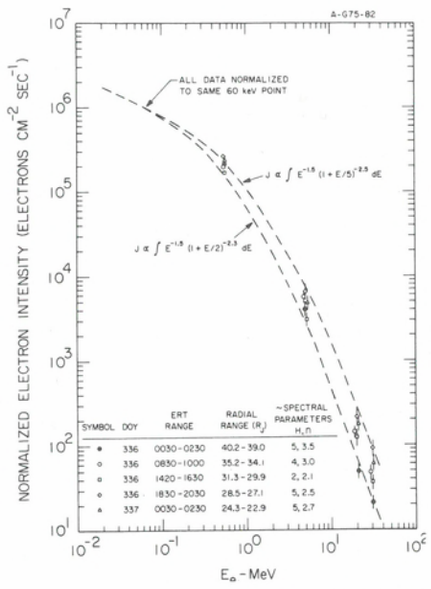

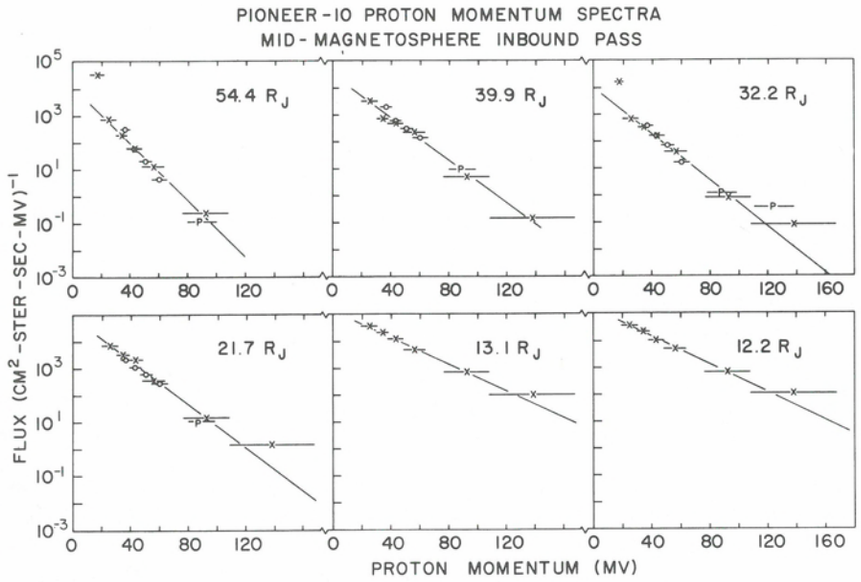

Fig. 5.9. (*a*) Electron spectra in the middle magnetosphere, 22–40 R_J, observed with the University of Iowa experiment on Pioneer 10-in. See Equation (5.8) for meaning of H and n [from Baker and Van Allen, 1976]. (*b*) Proton momentum spectra (1-hr averages) from the inbound pass of Pioneer 10 [from McDonald, Schardt, and Trainor, 1979; GSFC/UNH experiment].

a flux enhancement of 30% to 70% was observed at the 310° crossing [Vogt et al., 1979a]. The maxima in the Pioneer 10-in proton flux occurred one to two hours after the equatorial crossing, based on magnetometer data, also indicating a longitudinal component to the flux modulation. However, no longitudinal dependence was found in the Voyager 2 data (Fig. 5.8). A longitudinal effect may not always be found because

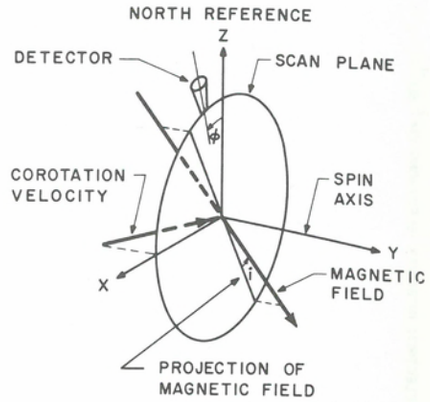

Fig. 5.10. Geometry of angular distribution measurements. The circle illustrates the path of the detector as the spacecraft (Pioneer) or as the scan platform (Voyager) turns about the y axis. The directions shown for the magnetic field and corotation velocity are typical of the Pioneer inbound passes.

any longitudinal dependence in particle source strength is averaged out by curvature and gradient drifts, provided particles remain trapped for several drift periods.

The differential spectra of energetic particles do not obey a simple power law in energy, but become steeper at higher energies. Below 0.5 MeV, the electron spectrum is an exponential in energy (Chap. 4), above 0.5 MeV it (Fig. 5.9*a*) can be represented by

$$j_e(E) = C E^{-1.5} \left(1 + \frac{E}{H}\right)^{-n} \tag{5.8}$$

where C, H, and n are free parameters [Baker and Van Allen, 1976; for a different representation, see McIlwain and Fillius, 1975]. In the middle magnetosphere, $5 \leq H \leq 35$ MeV and $2 \leq n \leq 5.5$. The off-equatorial spectra are somewhat softer than the equatorial spectra. As discussed in Chapter 4, the differential energy distribution of protons below 0.5 MeV is well described by a Maxwellian spectrum plus a high energy tail that follow a power-law distribution. However, proton spectra above 0.5 MeV are best expressed with an exponential dependence on momentum (Fig. 5.9*b*)

$$j(E) = \frac{C}{\sqrt{E}}\, e^{-\sqrt{E/E_o}} \tag{5.9}$$

where E_o corresponds to the e-folding momentum. This momentum falls into the range from 7 to 14 MV, or E_o equals 25 to 100 keV [McDonald, Schardt, and Trainor, 1979]. As in the case of electrons, the hardest spectra occur at the magnetic equator and there is little dependence of E_o on radial distance. Departures from the average shape of the proton spectrum have been observed and will be discussed later. Ion spectra have been observed primarily at energies below 0.5 MeV/nuc [Hamilton et al., 1981] and are discussed in Chapters 3 and 4.

Information about the magnetosphere can be derived from the angular distribution of the energetic particles. Angular distributions at Jupiter have been observed in a scan plane. During the Pioneer passes, this plane was nearly perpendicular to the ecliptic plane, it was generally parallel during the Voyager passes (Figs. 4.1 and 4.2). The orientation of the magnetic field, **B**, relative to the plane affects the type of information that can be derived (Fig. 5.10). If **B** makes an angle i with the plane, then only pitch angles in the range i to 180-i are sampled, and each pitch angle is sampled at two gyrophases. The angular distributions have been subjected to Fourier analysis in the form

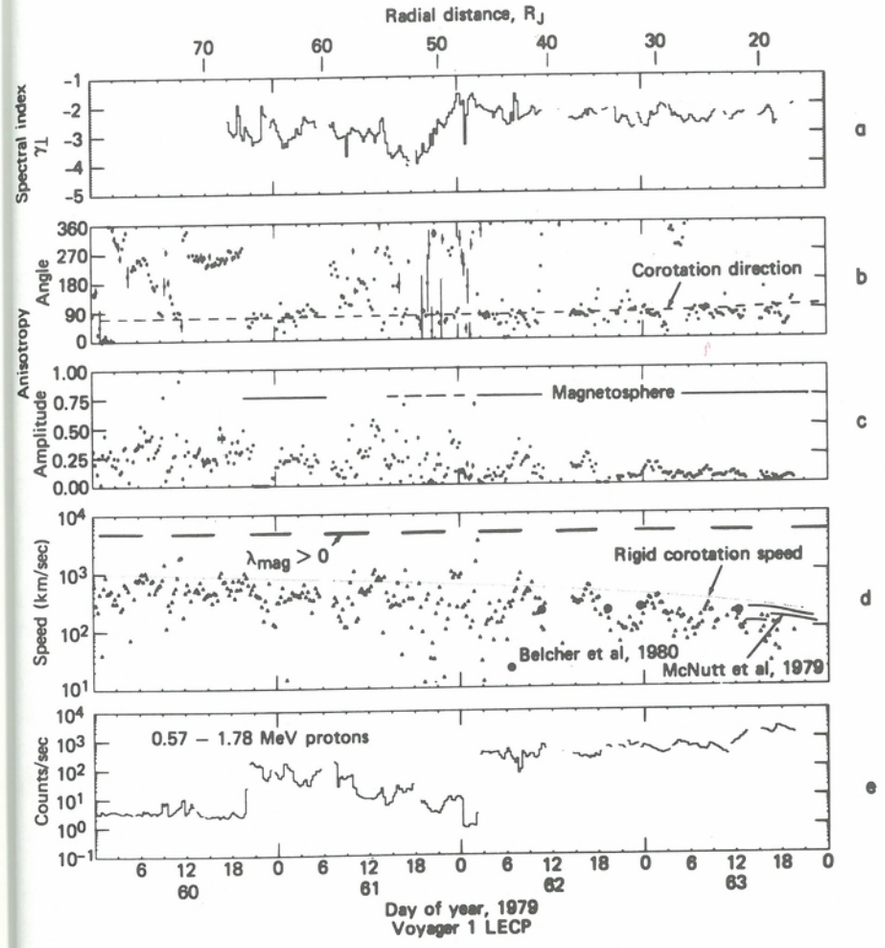

Fig. 5.11. Plasma speed derived from Compton–Getting effect of 0.57- to 1.78-MeV protons observed during the inbound pass of Voyager 1 with the Applied Physics Laboratory/University of Maryland Experiment: (*a*) Index of power law fit, $E^{-\gamma}$, to proton spectra; (*b*) Magnitude of first-order anisotropy; periods when the spacecraft was in the magnetosphere are identified with the solid line; (*c*) Direction of first-order anisotropy; the lines show the corotation and radial outflow directions; (*d*) Plasma speed with the speed for rigid corotation shown by the light line. Periods during which the spacecraft was in the northern magnetic hemisphere are given by bars along the top. Selected values of the plasma speed derived from the plasma experiment are shown by heavy dots [Belcher, Goertz, and Bridge, 1980; McNutt et al., 1979]; (*e*) Counting rate of 0.57- to 1.78-MeV protons [from Carbary et al., 1981].

$$j(v,\phi) = A_o(v)\,[1 + A_1/A_o \cos(\phi - \phi_1) + A_2/A_o \cos 2(\phi - \phi_2) + \ldots] \tag{5.10}$$

In this expression, $j(v,\phi)$ is the flux of particles with a given velocity entering the detector from the direction ϕ (Fig. 5.10). $A_o(v)$ is the spin averaged flux and A_n is the n^{th} order anisotropy. The even terms ($n = 2, 4, \ldots$) reflect primarily the pitch angle distribution for trapped particles. The odd terms reflect the effects of intensity gradients, of electric fields or the equivalent motion of the reference frame, and of field-aligned flow of the particle population.